WIND TUNNEL TESTING OF A FULL SCALE HELICOPTER BLADE SECTION WITH AN UPSTREAM ACTIVE GURNEY FLAP

R. Loendersloot[(1)] J. Freire Gómez[(2)] J.D. Booker[(2)]

[(1)] Applied Mechanics, Faculty of Engineering Technology, University of Twente, Enschede, The Netherlands, r.loendersloot@utwente.nl
[(2)] Department of Mechanical Engineering, University of Bristol, United Kingdom

ABSTRACT
Wind tunnel tests were performed on an aerofoil section comparable to that of a full scale helicopter blade section with an upstream active Gurney flap in the framework of the European project CleanSky ITD Green RotorCraft. A modified NACA0012 profile was used, with 23 Kulite pressure transducers embedded in the profile's surface and with an integrated actuator system for the Gurney flap. The Gurney flap, positioned at 95% of the chord length and with a deployed size of 1.3% of the chord length, extended the full span width of the section. The aerofoil was supported by a mounting system with automated control of the angle of attack. The effect of the Gurney flap is assessed for various deployment strategies. The test campaign carried out was successful. The aerodynamic behaviour can be extracted from the data and contains valuable information for validation of 2D numerical models developed by other partners in the project. The most important improvement of the setup for future use is the stabilisation of the inclinometer readings, which showed a significant amount of noise.

1 INTRODUCTION

In 2008, the JU Clean Sky ITD Green RotorCraft (GRC) project commenced, aiming at an improvement of the flight performance of helicopters in terms of fuel consumption and noise pollution. The research of Work Package 1, Innovative Rotor Blades, focussed on active strategies, such as active twist of the blade (DLR and Airbus Helicopters), laminar flow technology (CIRA) and the Active Gurney Flap system (AgustaWestland/IGOR). The latter research is conducted by a consortium of Benelux companies, for this specific part in collaboration with Microtecnica and the University of Bristol and supervised by AgustaWestland and is the subject of this paper.

One of the key milestones in this development is the validation of the 2D aerodynamic models that set the requirements for the design of a full scale active Gurney flap (AGF) system that is anticipated to be tested in flight at the end of the project. The Gurney flap has received a substantial amount of attention, reflected by the review from Wang *et al.* [1]. A relatively recent article from Cole *et al.* [2] proves the continuation of research efforts addressed to Gurney flaps and adds a relevant conclusion, after having analysed the performance of Gurney flap of various heights and for various airfoils: "*In summary, caution must be exercised when assuming the effects of the Gurney flap based on its height and location for an airfoil that has not been analyzed or measured*". The airfoil used in this research is based on the NACA0012 profile, which has been measured, amongst many others by Li *et al.* [3]. However, the majority of the research conducted is based on a static Gurney flap, located at the trailing edge, rather than at some point close to the trailing edge. The position of the Gurney flap is a practical implication if retraction is required as is the case for the active Gurney flap under investigation. Hence, it can be concluded only limited information on the dynamic behaviour, induced by the deployment and retraction phases, is available in literature for this airfoil. This directly results in the need to experimentally investigate the dynamic behaviour of the active Gurney flap by means of wind tunnel tests.

The tests were performed by a consortium of partners, each contributing a specific part to the test. The wind tunnel tests are carried out at the University of Twente, The Netherlands. The wind tunnel and test section, specifically designed for these measurements, are discussed in section 2, the profile, manufactured by Airborne Technology Center with an integrated AGF system designed and built by Microtecnica and the University of Bristol, is discussed in section 3 and the data acquisition, supported by the NLR, in section 4. The results acquired during the test are presented and discussed in section 6, while the paper is closed with conclusions and future prospects (section 7).

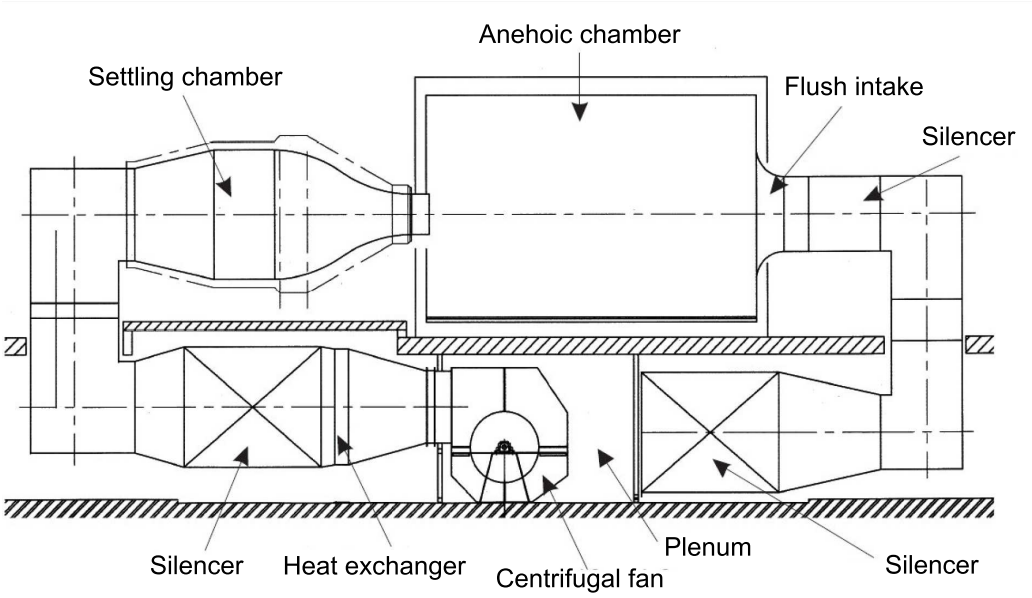

Figure 1: *Schematic overview of the wind tunnel of the University of Twente.*

2 WIND TUNNEL FACILITIES

The wind tunnel of the University of Twente, owned by the Chair of Engineering Fluid Dynamics, is a silent subsonic wind tunnel. It is used for both aerodynamic and aero-acoustic research. The tunnel has an open end test section of $0.9 \times 0.7\,\mathrm{m}^2$, placed in an anechoic room of $6 \times 6 \times 4\,\mathrm{m}^3$. A schematic overview of the tunnel is shown in figure 1.

The maximum wind speed that can be reached is approximately $58\,\mathrm{m\,s^{-1}}$ ($\sim$0.17 Mach). The tunnel is not pressurized and has a stream turbulence of 0.5-0.6%. In principle, isothermal conditions apply, but the temperature can increase during operation of the wind tunnel, depending on the conditions of the test and the equipment in the anechoic room. An uncontrolled cooling system can be used to reduce the temperature if desired.

The aerofoil that is tested (see section 3) has a relatively large chord length (0.508 m) compared to the tunnel dimensions. On top of that, the angle of attack has to be controlled accurately. The University of Twente has therefore developed a new test section with an integrated mounting system for the aerofoil. The new test section was placed behind the existing test section, though it can also replace the existing test section.

The first function of the mounting system is to define the position of the blade, without interrupting the flow (maximum gap of 0.5 mm) and assuring its alignment to be perpendicular to the flow. Furthermore, the blade has to be oriented horizontally in the span direction. The second function of the system is to control the angle of attack of the profile with an accuracy of 0.1° over a range of -5° to $+20^{\circ}$, while measuring it with an accuracy of 0.01°. The final function of the system is to absorb vibrations due to the operation of the AGF system (0 - 35 Hz)

The test section is made from plywood, for reasons of cost and for ease and flexibility of manufacture. An aluminium disc and ring system is manufactured to meet the requirements on accuracy. The assembly of the system, viewed from the outside is shown in figure 2.

The assembly consists of *i)* a ring for the alignment of the entire rotating system; *ii)* a disc base rotating in the ring, *iii)* a disc frame containing the mounting points for the aerofoil section; *iv)* three POM bearing blocks assuring the alignment and smooth and low friction rotation of the disc base in the ring; *v)* an inclinometer (Seiko N3 capacitive, liquid based) measuring the angle of the disc; and *vi)* a linear actuator (Transmotec DLA-24-40-A-200-POT-IP65) controlling the angle of the disc. The ring, disc base and disc frame are all manufactured from aluminium (6082 series). Both the inclinometers and the linear actuators require a power source. Stable regulated 5 Volt power is realised using a small circuit with a capacitor to stabilise a rectified power supply. The 24 Volts (direct current) for the linear actuators is generated with a separate power supply.

The gap between the aluminium alignment ring and the plywood is filled with filler material, whereas the gap between the rotating disc and the alignment ring is minimised by setting appropriate machining tolerances. As a result, a smooth, flush surface is obtained on the inside of the wind tunnel. The alignment of the disc in the rings is achieved by using adjustable POM sliding blocks. A detailed view of the assembly of the ring and disc in the plywood test section wall is given in figure 3.

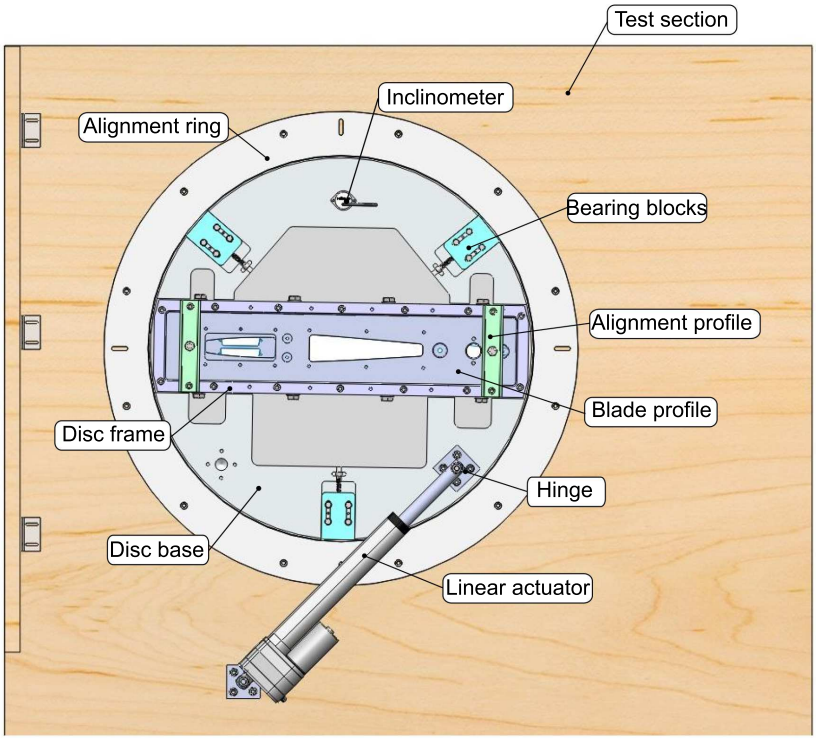

Figure 2: *Side view of the test section showing the mounting system for the rotor blade, which allows for an automatically controlled setting of the angle of attack of the rotor blade section.*

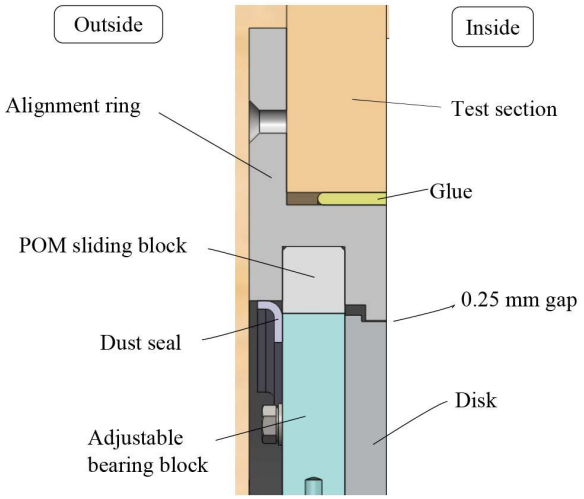

Figure 3: *Detailed view of the assembly of the outer, non-rotating aluminium ring and the rotating aluminium disc in which the rotor blade section is mounted. The adjustable bearing block allow for a precise and smooth rotation.*

An in-house developed LABVIEW© control program is employed to control the linear actuators, using the readings from the inclinometers as inputs. The two linear actuators on each side have to ensure the discs rotate simultaneously, with an accuracy of 0.1°. The LABVIEW© program adjusts the power sent to each of the linear actuators depending on the difference between the inclinometer readings and the target angle of attack set by the user. A screenshot of the LABVIEW© control program is shown in figure 4. The LABVIEW© program accounts for a minimum voltage required for operating the linear actuators and reduces the power if the current angle is within 1.0° from the target angle. The actuation stops if either the target angle is reached, within the preset accuracy, or if the difference between the readings of both inclinometers exceeds 1.0°. Unfortunately, it turned out to be impossible to use a lower value for this, due to a large amount of noise on the signal. This issue will be further addressed in section 6.

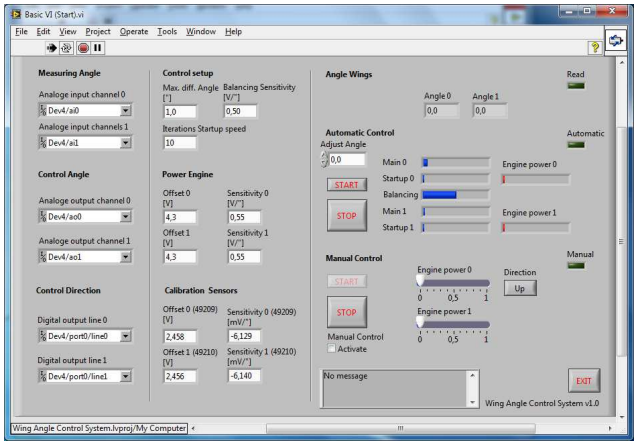

Figure 4: *Screenshot of the* LABVIEW© *control program*

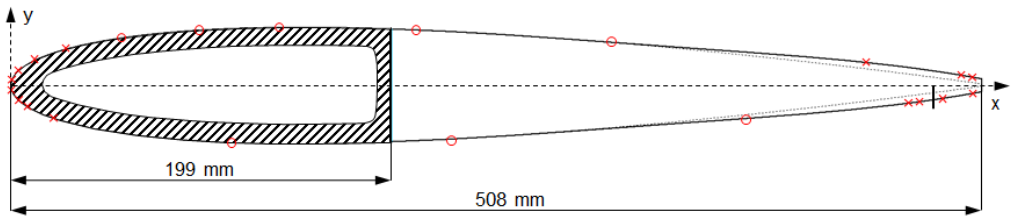

Figure 5: *Modified NACA0012 profile. The main dimensions are indicated. The dotted line indicates the original NACA0012 profile.*

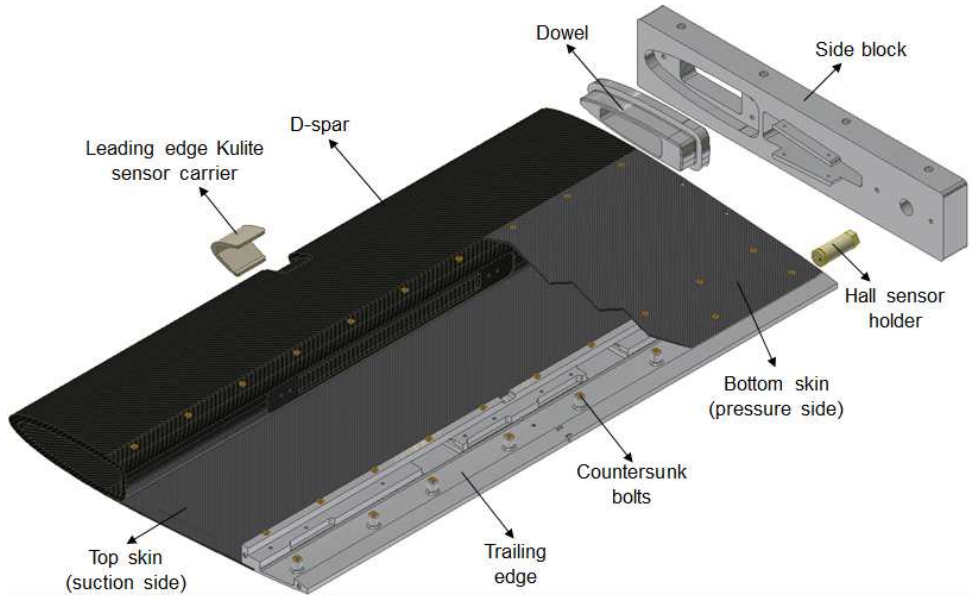

Figure 6: *Exploded view of the blade aerofoil section without the AGF mechanism.*

3 BLADE AEROFOIL SECTION AND AGF

The blade aerofoil section used for the wind tunnel test is a variant of the NACA0012, where the trailing edge has been thickened to provide greater spatial envelope for the AGF. The variant in question is characterised by having a 3% chord thickness at 95% chord (figure 5), and will be henceforth referred to as NACA0012M, where the 'M' stands for modified.

Airborne Technology Centre (The Hague) was responsible for the construction of the 900 mm wide blade section. This was designed so that the deformations at any point throughout it would be less than 0.1 mm during the test, thus ensuring the blade preserves its original shape.

Due to manufacturing constraints and in order to facilitate the installation of the AGF mechanism inside it, the blade section was broken down into different parts for manufacturing (see figure 6). The hollow D-spar was made out of prepreg IM7 Carbon/BMI resin, using the so-called Same Qualified Resin Transfer Moulding (SQRTM) method, which eliminates the need for an autoclave. The D-spar was then CNC milled to match its prescribed span-wise length, as well as to produce the cut-out for the cradle (see figure 8), the front pocket for the Kulite sensor carrier and the holes for both the bolts and Kulite sensors. The top and bottom skins of the aerofoil were also made out of prepreg IM7 Carbon/BMI resin, but using a standard manufacturing method (i.e. shaping them on female moulds, vacuum bagging them and curing them in an autoclave at approximately 6 Bar and 190°C). Both skins were later machined to match their prescribed span-wise length, as well as to produce the holes for the Kulite sensors and countersunk bolts (only in the case of the latter). The leading edge Kulite sensor carrier was rapid prototyped in Tusk XC2700 by Materialise (Leuven). Finally, the trailing edge part, the dowels and the side blocks were all machined out of solid aluminium.

Prior to proceeding to assemble the blade section parts, the outer surfaces of the D-spar, the Kulite sensor carrier, the skins and the trailing edge were all sprayed with non-reflective black paint, in order to enable the later use of the particle image velocimetry (PIV) system during the wind tunnel test. After this, the Kulite pressure sensors positioned around the mid-span section of the blade were installed on the individual parts. This process was carried out by Ext-Ins Technologies (The Netherlands). Due to the delicacy and very small size of these sensors, pro-

tective packagings had to be specially designed for them in order to facilitate installation (see figure 7). These protective packagings were rapid prototyped in polyamide by Shapeways (Eindhoven). The distribution of the 23 Kulite sensors around the mid-span section of the aerofoil (12 on the suction side and 11 on the pressure side) is shown in figure 5, where the red 'x' and 'o' points indicate the position of the LQ-062 Series and LL-250 Series sensors respectively. The precise chord-wise position coordinates for these may be found in table 1.

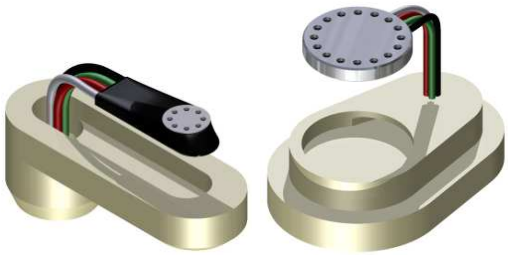

Figure 7: *Left: Exploded view of an LQ-062 Series Kulite pressure sensor and its protective packaging; Right: Exploded view of an LL-250 Series Kulite pressure sensor and its protective packaging.*

Table 1: *Chord-wise position (in mm) of the Kulite pressure sensors.*

Upper skin		Lower skin	
Sensor Id	Position	Sensor Id	Position
1	0.4	13	0.5
2	4.1	14	4.0
3	12.3	15	8.9
4	29.0	16	22.4
5	58.0	17	115.8
6	98.7	18	231.2
7	140.9	19	385.3
8	212.4	20	470.5
9	314.8	21	476.5
10	448.0	22	488.6
11	498.0	23	504.0
12	504.0		

Once the Kulite sensors had been installed, the top skin of the aerofoil was bonded to both the D-spar and the trailing edge using Araldite 2015, a two component adhesive. The Kulite sensor carrier was also attached to the D-spar using the same compound. After installation of the AGF inside, the blade section was closed by bolting the bottom skin to both the D-spar and the trailing edge part. Finally, the heads of the countersunk bolts (see figure 6) were covered with filler dough to eliminate any rough spots on the blade's outer surface that could disturb the flow.

Within the wind tunnel, the blade section is firmly held in place through two side blocks (see figure 6). Each of these has a pocket for a dowel which slides into the D-spar, the heaviest and stiffest part of the blade, thus providing the main supporting point. Extra support is provided through two protruding lips to which the aerofoil skins are bolted. The side blocks also house the Hall sensor holders, rapid prototyped in ABS plastic by the University of Bristol. The Hall sensors are used to measure the deployment height of the flap and provide a roughly linear voltage versus position output signal. The calibration of the voltage versus position characteristic of the sensors was carried out in situ once the blade aerofoil section had been installed within the wind tunnel.

The AGF was designed and manufactured jointly by Microtecnica (Turin) and the University of Bristol. The system was designed so that the flap sits at 95% chord and its deployment path is essentially perpendicular to the chord length (see figure 5). Using this configuration, the maximum achievable flap deployment height is 1.3% chord, although the system has capability for partial deployment and hold.

The topology for the AGF mechanism was selected following the methodology presented in [4]. A design based on flexures came out as the strongest candidate as these present a series of advantages over conventional joints: they are easily customisable, lightweight, maintenance free, backlash free (thus allowing precise control of the position) they do not produce friction losses and they eliminate the possibility of a jam during motion [5].

The selected topology is shown in figure 8. It consists of a CFRP cradle which houses the actuator, a push-rod that transfers the movement from the leading edge to the trailing edge, and a flap hinging on flexures. These are in turn anchored to a series of rail segments which are bolted to the trailing edge part shown in figure 6.

In order to make sure that the flexures would have infinite fatigue life, a high ultimate strength spring steel was selected (CS95 (EN44)). The thickness was chosen using the relation for the endurance limit σ_e of the material in question (550 MPa), which according to [6] reads:

$$\sigma_e = \frac{(3\lambda - 1)Et\theta}{L} \tag{1}$$

Where λ is a non-dimensional parameter which defines the point at which the flexures cross relative to their length (1.06), E is Young's modulus (200 GPa), t is the flexure thickness (0.127 mm), θ is the angle across which the flexures move ($\pm 5^{o}$) and L is the active length of the flexures (9.4 mm). The span-wise width of the flexures, which has no influence on the stress levels, was taken as 45 mm. It is also worth pointing out that the flap is partially deployed when the flexures are at their neutral position, as can be inferred from figure 9, in order to keep the absolute

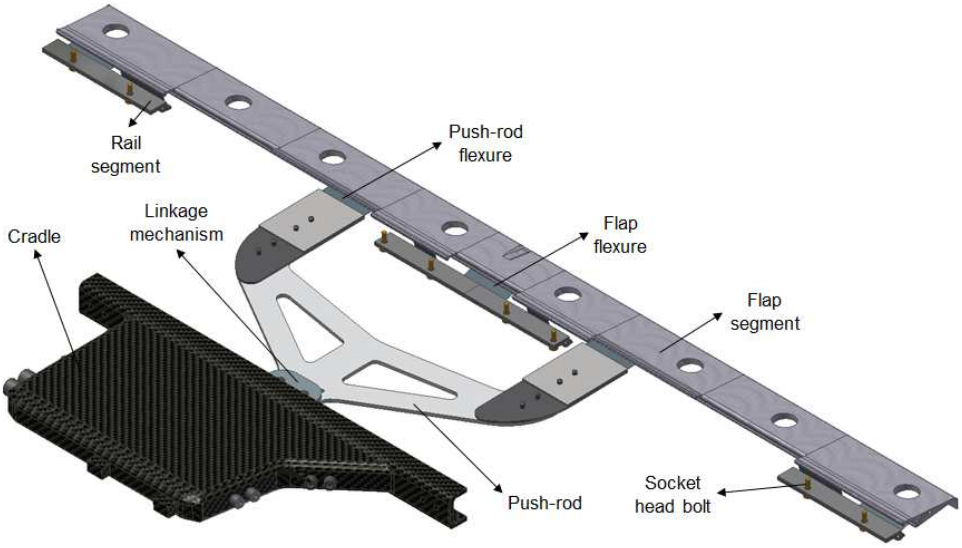

Figure 8: *Isometric view of the AGF mechanism.*

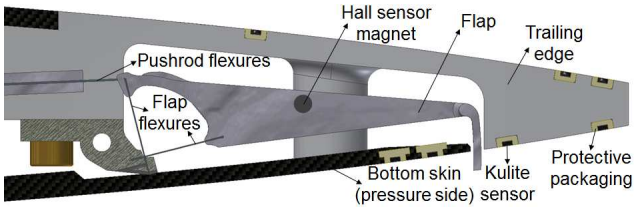

Figure 9: *Side view of the flap showing the cross-axis flexural pivot.*

angle across which the flexures move to a minimum. In other words, the flexures have a -5° angular rotation when the flap is fully stowed inside the blade, whereas they reach a +5° angular rotation when the flap is fully deployed.

Before committing to manufacture of the actual test parts, the design was thoroughly validated both analytically through FEA as well as through experimental prototype testing. Two bench tests were performed: one using a scanning laser Doppler vibrometer (SLDV) to verify that the flap did not possess any natural frequencies close to the frequency range during testing (0-35 Hz) and that it had an even deployment across its span during operation; and another one to test the fatigue life of the flexures, subjecting them to 10^7 cycles with a motion range covering the maximum flap deployment height.

Due to manufacturing constraints, the 900mm long flap had to be divided into nine shorter segments which were machined out of solid aerospace grade aluminium using wire-EDM. These segments were then assembled together on a surface table using dowels and Loctite 278 (a thread locking high strength adhesive), thus ensuring perfect straightness of the flap. To enable the use of the PIV system during the wind tunnel test, the flap tip was sprayed with non-reflective black paint. The rail segments and push-rod plates were also made out of aluminium using wire-EDM. Once the flexures, the flap and the rail segments had been glued together using the aforementioned adhesive, the latter were then bolted to the trailing edge part shown in figure 6 and figure 9. Lastly, the push-rod was connected to both the linkage mechanism and the push-rod flexures using socket head bolts and nuts.

4 DATA ACQUISITION

The data acquisition of most parameters was done under supervision of the NLR, using their VIPER data acquisition system. The aerodynamic pressure, measured by the 23 Kulite sensors, the sound pressure at the top and bottom wall of the test section (8 LinearX M51 microphones), the position of the Gurney flap (2 Hall sensors), the readings of the inclinometers (also input of the LABVIEW© control program), and the temperature in the D-spar (Omega Thin Film RTD PT1000) and the accelerations of the Gurney flap were all recorded by the VIPER system.

A second PC was used to store *i)* the data from the two inclinometers, imported via a NI myDAQ system; *ii)* the data from two thermocouples in the original test section of the wind tunnel to measure the temperature of the airflow; *iii)* 10 static pressure tabs integrated in the top wall of the test section; and *iv)* the air flow velocity, based on a pitot tube (2 channels). All pressures, including those from the pitot tube are measured by a NUSS system.

The PC was also used to control the actuation, which operated on a different circuit: it had its own power supply and the temperature of actuator was measured to avoid overheating.

The VIPER system allows 48 different channels to be connect, of which 40 were used. The front of the

VIPER system is shown in figure 10. The VIPER has 6 modules, each holding 8 channels. Various types of connectors can be used (BNC / LEMO / SubD), a current of up to 4 mA can be supplied as well as a direct current power supply of 5, 10, 12 or 15 Volts. The maximum sampling frequency is 200 kHz and an on board signal amplification can be used. The data files are stored as FAMOS binary files, allowing for extreme large data binary files ($\gg$1 Gb). The sampling frequency for most cases was set to 40 kHz, only a few of the first measurement were sampled with 20 kHz.

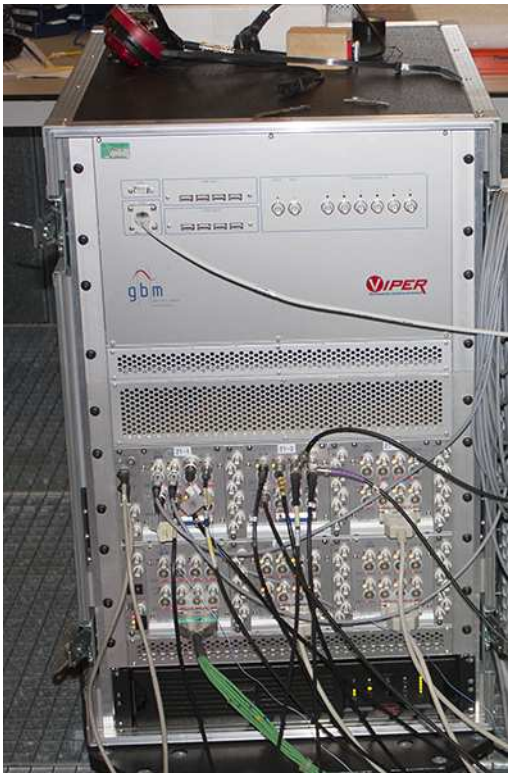

Figure 10: *Front view of the* VIPER *data acquisition system.*

The parameters measured are collected in table 2. All Kulite pressure transducers were connected to the VIPER with SubD connectors. Hence, a multiple of 8 channels was used, leaving one redundant channel. BNC connectors were used for all other data channels.

The wires from the Kulite pressure transducers are extremely fragile. Any handling or operation can cause breaking and a consequent loss of the signal. Therefore, the wires were carefully led from the center of the profile to the sides, while supporting them on strategic locations, where they were connect to a male SubD connector. The connectors were attached to the side blocks (see figure 6). Once installed, the wires were completely protected against handling operations during installation of the set up in the wind tunnels as well as operations during the tests such as setting the angle of attack. Moreover, the test section and the VIPER data acquisition system were easily connected using a SubD cable.

Table 2: *Overview of data acquisition.*

Type	Number	System
Kulite – Dynamic pressure		
LL-250 0.7 bar A	9	VIPER
LQ-062 0.7 bar A	14	VIPER
LinearX – Acoustic pressure		
M51	8	VIPER
NUSS – Static pressure		
Pressure tubes	10	UT-PC
Temperature		
RTD Pt1000	1	VIPER
Position		
Hall sensors	2	VIPER
Accelerometers	4	VIPER
Seiko N3 Inclinometers	2	VIPER/UT-PC

The angle of attack is measured by two Seiko N3 inclinometers, serving as the input for the LABVIEW© program that is used to control the motion of the linear actuators. The inclinometers have a measuring range of $\pm 30^{\circ}$ and a resolution of less than $5{\cdot}10^{-3}\ ^{\circ}$. The sensors require a regulated 5 V supply voltage. A small electrical circuit is built, shown in figure 11, to convert and stabilise an AC voltage to a regulated supply voltage of 5 V. The measured voltage V and the angle α of the inclinometer are linearly related (0.2% deviation over measuring range) according to the data sheet provided by the supplier of the inclinometers. The relation is given for each sensor separately as:

$$V_{\text{right}} = 2.490 - 6.129 \cdot 10^{-3}\alpha \qquad V_{\text{left}} = 2.498 - 6.140 \cdot 10^{-3}\alpha \tag{2}$$

The subscripts 'right' and 'left' are with respect to the flow direction.

The inclinometers signals are used by the LABVIEW© program, but also read by the VIPER, as they are used to determine the actual angle of attack. The wires were therefore split, which resulted in a different reading in the LABVIEW© program, most likely caused by differences in the internal resistances of the VIPER and the NI myDAQ, combined with different (and long) wires. The readings the two inclinometers changed approximately an equal amount in opposite direction.

The sensitivity parameters were adjusted by applying a constant shift. The shift appeared sufficient for a correct operation of the disc rotation system up to 10°. The corrected sensitivities were found to be:

$$V_{\text{right}} = 2.433 - 6.129 \cdot 10^{-3}\alpha \qquad V_{\text{left}} = 2.431 - 6.140 \cdot 10^{-3}\alpha \tag{3}$$

Note that the sensitivity factors are adjusted with

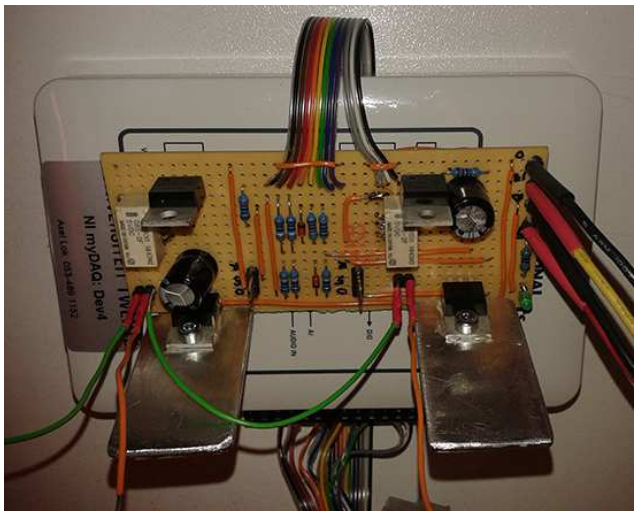

Figure 11: *Supply voltage regulator for the inclinometers, positioned on top of the NI myDAQ data acquisition unit.*

a constant term; the linear coefficients were not changed.

5 TEST PLAN

Four different test phases were defined:

1. Static deployment
2. Oscillatory deployment
3. Ramped deployment
4. Ramped deployment/wake

The last is partly a repeating of the measurement of the third phase, but the PIV was focussed on the wake rather than on the area around the Gurney flap. The reader is referred to the paper of Van 't Hoff *et al.* [7] for the results of the wake measurements.

The test matrix for each phase comprised a series of common variables, such as the range over which the angle of attack was varied (-2°–12°), the amount of deployment (0 mm/0%, 2.5 mm/0.5%, 5.1 mm/1%, 6.6 mm/1.3%) and the wind speed (30 m/s and 60 m/s). During the first phase, the maximum achievable deployment (7.2 mm/1.4%) was also included in the test matrix.

The Gurney flap was deployed with sine functions. Four different frequencies were used: 5 Hz, 10 Hz, 20 Hz and 30 Hz. The frequency must be scaled to be able to compare the deployment frequency with actual flight situations, due to the relatively low Mach number in comparison to the Mach number in real operation. The reduced frequency k is calculated to this end by:

$$k = \frac{\omega L}{2V} = \frac{\pi f L}{V} \tag{4}$$

with ω the circular frequency in radians per second, f the circular frequency in Hertz, L the chord length of the profile and V the flow velocity. However, the deployment schedules have not been chosen such that they can be compared directly with realistic operational conditions, but were merely chosen to push the envelope and investigate the limits of performance of the system.

The ramped deployment contained four phases: *i)* deployment; *ii)* a deployed region; *iii)* retraction and *iv)* a retracted position of the Gurney flap. The resulting schedule is shown in figure 12. The speed of deployment and retraction was varied, using four different values (21.667 ms, 25.000 ms, 19.444 ms, 13.333 ms). It was not possible to change the total time of a deployment cycle, due to constraints in the actuator control software. In order to be able to continuously repeat the schedule, the deployed time and retracted time was kept equal for all cases.

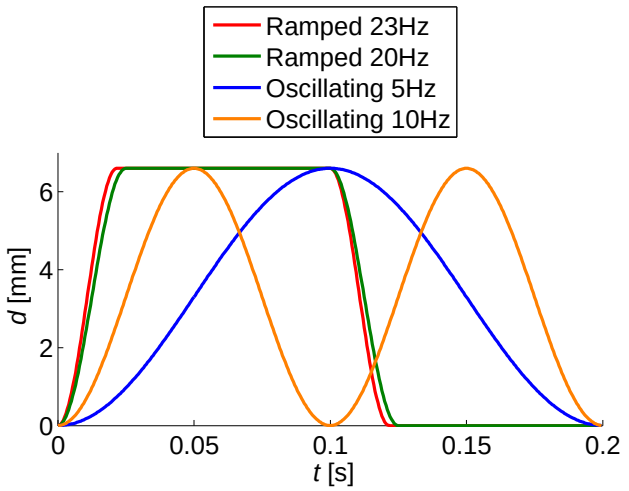

Figure 12: *The schedules for a ramped and oscillating deployment (two variations for each). The ramped deployment has four phases: the deployment, deployed region, retraction and stowed position.*

The angle of attack and the wind speed were set prior to each measurement, although a new angle of attack was set without stopping the wind tunnel. Each measurement lasted 30 seconds, after which just over 10 minutes of time was required to download the data from the PIV cameras and the next measurement could be started. The time between measurements was reduced to the time needed to set the conditions for the next measurement, possibly including loading a new deployment schedule, if no PIV measurement was included. A total of 222 measurements were performed (phase 1: 84; phase 2: 62; phase 3: 62; phase 4: 14), excluding a number of 'zero-measurements'. These measurements were done for calibration purposes of the Kulite pressure transducers. The wind tunnel was stopped completely during these measurements, resulting in an atmospheric pressure in the tunnel.

6 RESULTS & DISCUSSION

The amount of data generated is – the least to say – large. The objective of this paper is not to discuss all measurements in detail. The most important results from the wake measurement are, as mentioned, presented by Van 't Hoff *et al.* [7]. The analysis of the vibrations of the Gurney flap system will be presented by Dos Santos *et al.* [8] at the ISMA2014 conference in Leuven.

The discussion here covers the way the data is extracted and the most relevant observations. Firstly, the measurement of the angle of attack is discussed, followed by a discussion on the results of the lift coefficient, calculated from the dynamic pressure measurement. This discussion includes the effect of the Gurney flap on the lift coefficient. Subsequently, some observations concerning the Hall sensor data are discussed in relation to the targeted deployment schedules. Finally, preliminary results on the acoustic measurements are briefly touched upon.

6.1 Angle of Attack

The angle of attack is set via the LABVIEW© control program. However, the actual angle can deviate from the target angle. This is acceptable, since the inclinometer output is also read by the VIPER (as stated in section 4). Unfortunately, a significant amount of noise was observed in the signal from the inclinometers. As a consequence, it was not possible to control the difference in rotation angle of the discs with an accuracy of less than 1°. Moreover, connecting the inclinometers to both the LABVIEW© control system and the VIPER affected the sensitivities (see section 4). Hence, the signal is analysed in detail.

The first observation is that the inclinometer readings indicate a large difference between the angles of the both rotating discs. The angle of attack α, as measured by the both inclinometers during the full measurement period of 30 s, for a target angle of 8°, a fully retracted Gurney flap and a wind speed of 30 m/s is shown in figure 13a. Clearly, a significant amount of noise is present. The minimum and maximum values measured are also significantly larger than the maximum angle set by the LABVIEW© program during the motion cycle; once the rotation is stopped, there is no check anymore. Although the displayed measured values of the angles were far from stable, they appeared to vary significantly less than observed in the results displayed in figure 13. However, the signal as received by LABVIEW© was not stored and can therefore not be verified.

The second case shown in figure 13b is significantly more demanding for the mounting system: an oscillating Gurney flap deployment (6.6 mm at 30 Hz) and a higher wind speed (60 m/s). The histograms of both cases are shown in figure 14. The graphs show that the difference between left and right inclinometer is slightly larger for the second, more demanding case, but the standard deviation is slightly lower. Other cases show a similar trend. Hence, it can be concluded that the difference between the readings is relatively constant. It can therefore be stated that a reasonable approximation of the angle of attack at the mid span location, where the Kulite pressure transducers are located, is the mean value of the angles measured at both sides of the test section.

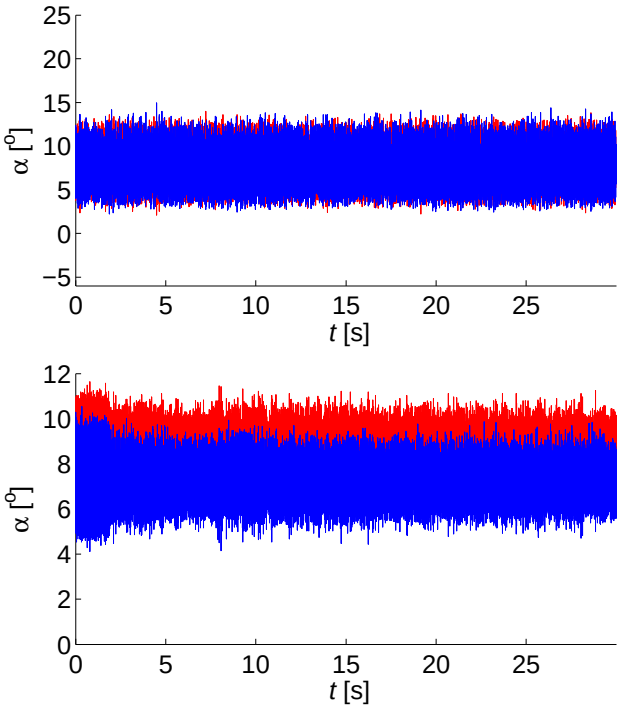

Figure 13: *Angle of attack (target: α=8°, red: right with respect to flow direction, blue: left). a): a fully retracted Gurney flap and a wind speed of 30 m/s; b) an oscillating Gurney flap deployment (6.6 mm at 30 Hz) and a wind speed of 60 m/s.*

6.2 Lift Coefficient

The lift coefficient was calculated using the dynamic pressures measured by the Kulite transducers. The profile is first discretised in elements, with the edge of the element in the middle of two neighbouring sensors. The leading edge and trailing edge points ($(x, y) = (0, 0)$ and $(x, y) = (L_c, 0)$) are also included. The pressure of each Kulite sensor is subsequently divided by the projected area of its element on either the local x-axis or the local y-axis. Hence, the resulting forces along and perpendicular to the chord length are obtained. These are subsequently rotated to the global coordinate system (X, Y) to obtain the lift and the drag coefficient. The latter is not considered here, as it is known to be inaccurate in these type of measurements. The lift coefficient $C_l$is defined as:

$$C_l = \frac{F}{\frac{1}{2}\rho v^2 L_c} \tag{5}$$

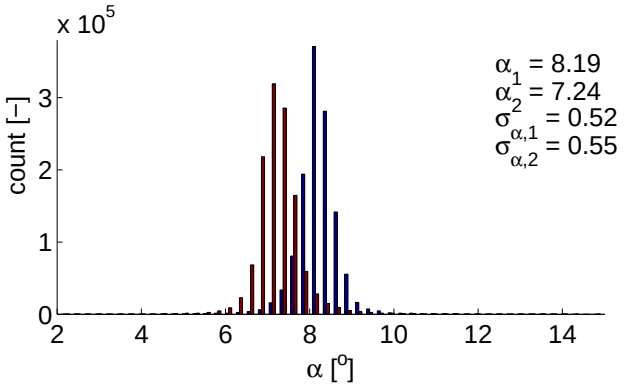

***a**: A fully retracted Gurney flap and a wind speed of 30 m/s.*

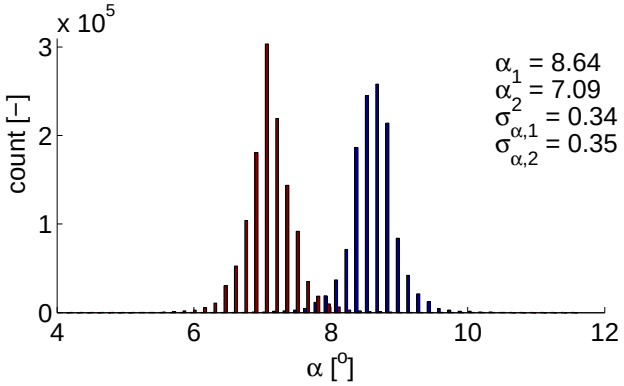

***b**: An oscillating Gurney flap deployment (6.6 mm at 30 Hz) and a wind speed of 60 m/s.*

Figure 14: *Histogram of the angle of attack (target: α=8°, red: right with respect to flow direction, blue: left).*

with F the force per unit length in span direction, ρ the density of air, v the relative velocity between profile and surrounding medium and L_c the chord length of the profile. The resulting lift coefficient for an angle of attack between -2° and 12°, a wind speed of 60 m/s and *i)* a fully retracted Gurney flap; *ii)* 2.5 mm (0.5%) deployment; *iii)* 5.1 mm (1.0%) deployment; and *iv)* 7.2 mm (1.4%) deployment is shown in figure 15. Note that a static deployment of the Gurney flap is used here and sufficient time was left between the measurement to obtain a quasi-static condition in the wind tunnel. The results are consistent with the expectations: a zero lift for a fully retracted Gurney flap and an overall increase of the lift for an increasing deployment of the Gurney flap.

It was also investigated if the oscillating operation of the Gurney flap results in time averaged change of the lift coefficient. The time averaged lift coefficient for three different actuation frequencies (5 Hz, 10 Hz and 20 Hz) are investigated to this end. The amplitude of the oscillation is also varied with three levels (2.5 mm, 5.1 mm and 6.6 mm). Note that a lower maximum deployment is used compared to the static deployment case, to limit the actuator forces. The lift coefficients for the 9 cases are shown in figure 16. The

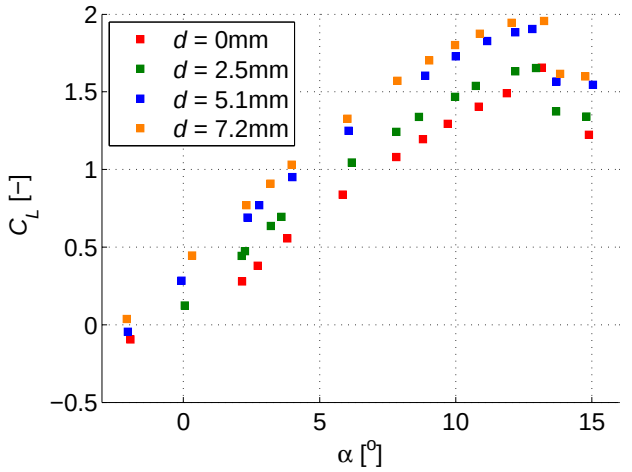

Figure 15: *The lift coefficient for four different static deployment levels of the Gurney flap for a wind speed of 60 m/s.*

value of the lift coefficient is not significantly affect by the sinusoidal deployment schedule. No relation can be established between the frequency of deployment and the lift coefficient, as there is no difference in the lift coefficient. This leads to the conclusion that the time averaged lift coefficient is not affected by the frequency of the oscillating deployment. However, the lift coefficient is, according the expectations, slightly lower compared to the lift coefficient in case of a static deployment.

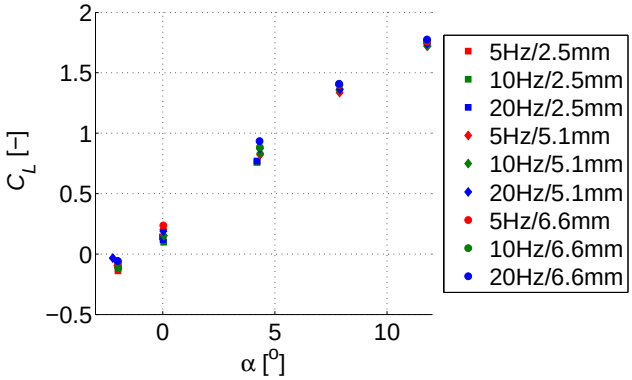

Figure 16: *The lift coefficient for three different actuation frequencies with each three different deployment amplitudes of the Gurney flap for a wind speed of 60 m/s.*

An oscillating deployment schedule will generally be chosen for vibration control rather than for increasing the flight performance. Hence, the change of lift is of limited value; it is more relevant that the operation does not change the performance too much. The associated increase of drag would therefore be as important as the change of the lift coefficient. As stated earlier, it is not possible to determine the drag coefficient accurately with these type of measurements.

6.3 Gurney flap position

In principle, the Gurney flap position is controlled by the deployment schedule applied to the actuator. The actual position of the Gurney flap can however slightly differ from the commanded position, due to flexibilities in the system. The actual position of the Gurney flap is compared with the commanded profile for different cases.

One of the main observations from this analysis is that the Hall sensor do not measure the position of the Gurney flap correctly close to the fully retracted position.

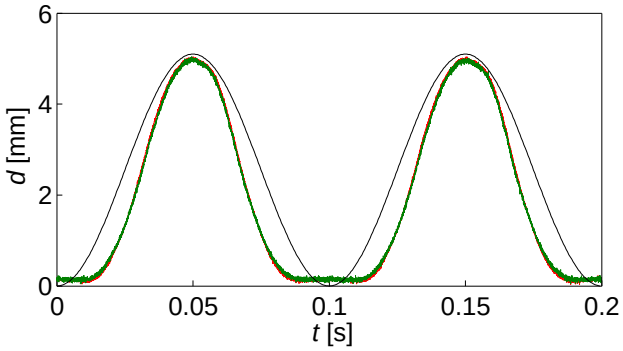

***a**: 10 Hz oscillating deployment frequency.*

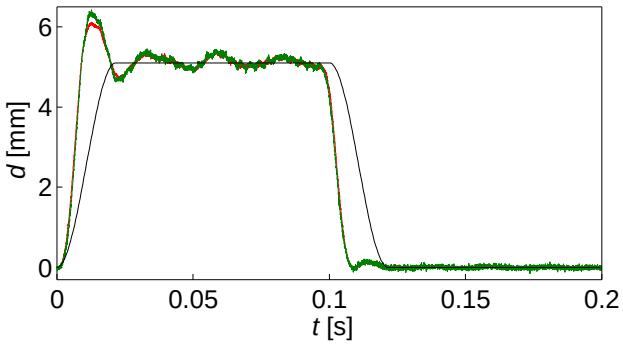

***b**: 23.077 Hz ramped deployment.*

Figure 17: *Comparison between the commanded deployment profile and the measured Gurney flap position.*

Secondly, it is observed that the Gurney flap accurately follows the motion of the actuator, if an oscillatory deployment is commanded, as shown in figure 17a, which shows the deployment measured by the Hall sensors compared to the commanded profile for a 10 Hz oscillating deployment schedule and a 5.1 mm amplitude of the deployment. There is no significant delay, even for cases with a relative high aerodynamic loading on the Gurney flap.

The difference between the commanded profile and the actual deployment are larger for the ramped case, shown in figure 17b. There is also a significant amount of overshoot present. It is not unknown whether the overshoot is caused by the actuator not being able to generate sufficient force for the required acceleration or by the flexibility of the push rod and GF system.

6.4 Acoustics

A total of 8 microphones where embedded in the top (6) and the bottom (2) of the wind tunnel test section, measuring the acoustic pressure. The objective of the acoustic measurement is to investigate whether it is possible to locate the disturbances introduced by the Gurney flap, using source localisation techniques and to estimate the extent of the disturbances by comparing the sound intensities of various situations. The analysis of the acoustic data is still in progress, but another observation, made during the measurements will be addressed here: specific combinations of angle of attack and Gurney flap deployment schedule resulted in a whistling sound. This sound was clearly audible outside the wind tunnel and hence it is expected that this shows up in the acoustic results.

The time dependent acoustic pressures are first transformed to the frequency domain, using an FFT analysis. The sampling frequency was sufficiently high (40 kHz in most cases) to obtain a sufficiently wide frequency band, but the time of measurement was relatively short: each measurement lasted 30 s. The number of points for the FFT analysis, N_{fft}, was chosen such that the frequency resolution was not larger than 1 Hz. This meant, each window contained 2^{16} data points, resulting in a frequency resolution of 0.62 Hz. Given the total length of the time signal and using an overlap of 50%, the resulting power spectral density was built with approximately 30 time windows.

The power spectral density of various cases is compared: first the case of no deployment is analysed, followed by the effect of an increasing angle of attack and some level of deployment of the Gurney flap. Finally, the effect of an oscillating deployment on the acoustic pressure is analysed.

The first case analysed is the fully retracted Gurney flap, 4° angle of attack and a wind speed of approximately 60 mm/s. The 0° angle of attack could not be analysed at this moment in time. The frequency range

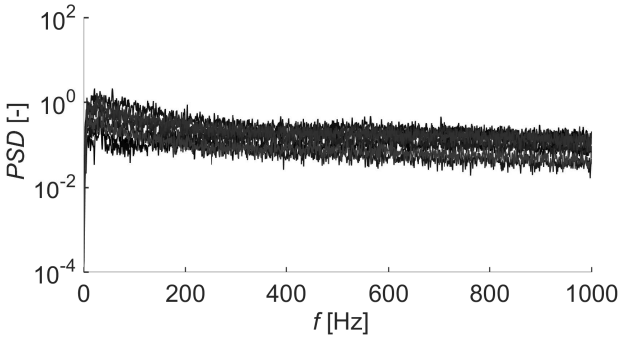

Figure 18: *Power spectral density measured by the 8 acoustic microphones for a fully retracted Gurney flap, an angle of attack of 4° and a wind speed of 60 m/s.*

The power spectral densities for a 4° angle of attack, harmonic oscillations of 5 Hz, 10 Hz and 20 Hz

and a deployment amplitude of 6.6 mm, depicted in figure 19, show an interesting change: the number of higher harmonics significantly increases for the faster deployment. The spectral density is also higher around 600 Hz. Clearly, the sound generated in those configurations is different and more tonal. The same characteristics are observed for other cases.

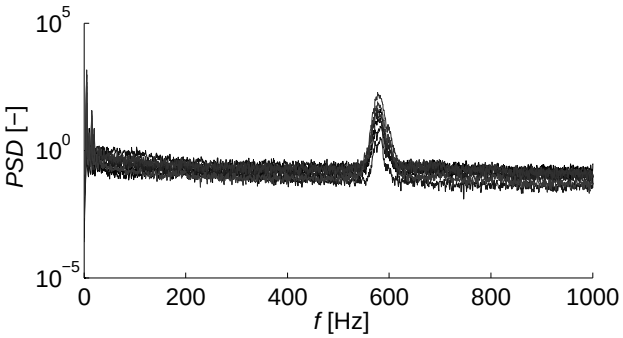

***a**: 5 Hz deployment frequency.*

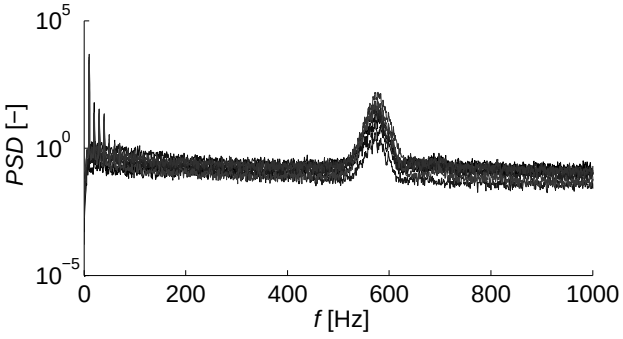

***b**: 10 Hz deployment frequency.*

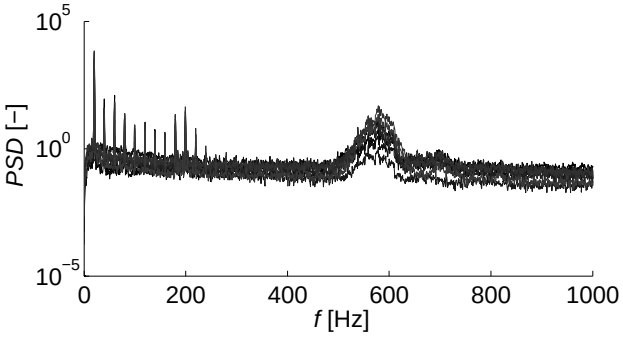

***c**: 20 Hz deployment frequency.*

Figure 19: *Power spectral densities for a 4° angle of attack, a wind speed of approximately 60 m/s and a Gurney flap deployment oscillation with an amplitude of 6.6 mm.*

7 CONCLUSIONS & FUTURE PROSPECTS

The wind tunnel test performed at the University of Twente, in the framework of the CleanSky project, required the collaboration of many partners from all over Europe. The test program ultimately aims to provide experimental data to validate the 2D aerodynamic models, as being developed by the NLR and AgustaWestland in this same European project. These models will then further support the design of a real Gurney flap, to be tested in flight at the end of the project. The main conclusion here, is that it is proven to be possible to successfully carry out a test campaign on a profile with components and a data acquisition system that were built or provided by different partners. This is a major challenge, both in terms of construction as in terms of coordination.

The measurements have not only just been successful, thanks to a good collaboration between the partners, but brought even more: the PIV measurements, described in the paper of Van 't Hoff *et al.* [7], were unique in the sense a mobile stereo PIV setup was used. The mounting system, specifically designed for this measurement, but such that it can be used for other profiles as well, provided the chord length and height of the aerofoil does not exceed the dimensions of the modified NACA0012 aerofoil used here. Also, the active Gurney flap system allowed for a unique assessment of the effect of different deployment schedules on the aerodynamics.

It was shown to be possible to assess the main characteristics of the presence of a Gurney flap on the aerodynamics, both for a static and an active deployment schedule (oscillating and ramped). A detailed analysis of all the data is still ongoing: the amount of data that is collected is large and various connection between different outputs can be made.

Still, there is a number of issues that demand further development. First of all, the noise on the signals, in particular on the inclinometer readings, has to be improved. The problem with the inclinometer readings was further increased by connecting the output signal to both the VIPER data acquisition system and the NI myDAQ system/LABVIEW© control program. Though this was essential to be able to set and measure the angle of attack, improvements are expected if the power supply of the inclinometers is further stabilised, the wires are shorted and isolated better from for example the actuator power supply. Finally, an additional calibration of the sensitivities is preferred, once the system is completely installed in the wind tunnel, taking into account all disturbing factors.

Secondly, the actuator control showed limitations. It is advised to control the design process of such a control system tightly. One of the main limitations was the time window of 200 ms for a deployment cycle. Though this corresponds approximately to one revolution of the type of helicopter that will be used for the flight test, it is an undesirable limitation for a 2D wind tunnel test; the relevant speeds, for example of the deployment, can be different due to the lower wind speeds.

Although it is unlikely that the measurements will be repeated, the recommendations can be valuable for comparable test campaigns. At this moment, the mounting system is being reconstructed for measurements on a wind turbine blade. This opportunity will broaden the experience with the mounting system and

be used to further develop the data acquisition and control of the angle of attack.

ACKNOWLEDGEMENTS

The authors wish to acknowledge Arjan Hanema, Jaap Cornelissen and Martijn Tuinstra from the NLR for their invaluable support in executing the tests, in particular regarding the data acquisition. Furthermore, Marco Zamboni (Microtecnica), Dario Arzelà (Microtecnica), Fabio Santos (LMS), Tjalling Stelma (Airborne) and Simon Spurway (Agusta Westland) are acknowledged for their support during the test and in the preceding phases. This project is funded by the CleanSky Joint Technology Initiative (grant number CSJU-GAM-GRC-2008-001) – GRC1 Innovative Rotor Blades, which is part of the European Union's 7th Framework Program (FP7/2007-2013).

REFERENCES

[1] J.J. Wang, Y.C. Li, and K.-S. Choi. Gurney flaplift enhancement, mechanisms and applications. *Progress in Aerospace Sciences*, 44:22–47, 2008.

[2] J.A. Cole, A.O. Vieira, and J.G. Coder. Experimental investigation into the effect of Gurney flaps on various airfoils. *Journal of Aircraft*, 50(4):1287–1294, July-August 2013.

[3] Y. Li, J. Wang, and P. Zhang. Effects of Gurney flaps on a NACA0012 airfoil. *Flow, Turbulence and Combustion*, 68:27–39, 2002.

[4] J. Freire Gomez, J.D. Booker, and P.H. Mellor. Design and development of an active gurney flap for rotorcraft. In *Proceeding of SPIE - The International Society for Optical Engineering*, volume Smart Structures/NDE, 2013. Paper 8690-15.

[5] L.L. Howell, S.P. Magleby, and B.M. Olsen. *Handbook of Compliant Mechanisms*. John Wiley and Sons, 2013.

[6] P. Xu, Y. Jingjun, Z. Guanghua, and B. Shusheng. An effective pseudo-rigid-body method for beam-based compliant mechanisms. *Precision Engineering*, 34:634–639, 2010.

[7] S. van 't Hoff, M. Tuinstra, and M. van Rooij. Time-resolved stereo PIV measurements of an active Gurney flap system. In *Proceedings of 40th European Rotorcraft Forum*, 2014.

[8] F.L.M. dos Santos, B. Peeters, Y. Lemmens, W. Desmet, and L.C.S. Góes. Experimental vibration analysis of a rotorcraft active Gurney flap system. In *Proceedings of the 26th ISMA conference – accepted as oral presentation*, 2014.